A&A 521, A5 (2010)
DOI: 10.1051/0004-6361/201014509

Astronomy & Astrophysics

Time, spatial, and spectral resolution of the Hα line-formation region of Deneb and Rigel with the VEGA/CHARA interferometer⋆

O. Chesneau[1], L. Dessart[2], D. Mourard[1], Ph. Bério[1], Ch. Buil[3], D. Bonneau[1], M. Borges Fernandes[1,9], J. M. Clausse[1], O. Delaa[1], A. Marcotto[1], A. Meilland[4], F. Millour[4], N. Nardetto[1], K. Perraut[5], A. Roussel[1], A. Spang[1], P. Stee[1], I. Tallon-Bosc[6], H. McAlister[7,8], T. ten Brummelaar[8], J. Sturmann[8], L. Sturmann[8], N. Turner[8], C. Farrington[8], and P. J. Goldfinger[8]

[1] UMR 6525 H. Fizeau, Univ. Nice Sophia Antipolis, CNRS, Observatoire de la Côte d'Azur, Av. Copernic, 06130 Grasse, France
e-mail: Olivier.Chesneau@oca.eu
[2] Laboratoire d'Astrophysique de Marseille, Université de Provence, CNRS, 38 rue Frédéric Joliot-Curie, 13388 Marseille Cedex 13, France
[3] Castanet Tolosan Observatory, 6 place Clemence Isaure, 31320 Castanet Tolosan, France
[4] Max-Planck Institut für Radioastronomie, Auf dem Hügel 69, 53121 Bonn, Germany
[5] Laboratoire d'Astrophysique de Grenoble (LAOG), Université Joseph-Fourier, UMR 5571 CNRS, BP 53, 38041 Grenoble Cedex 09, France
[6] Univ. Lyon 1, Observatoire de Lyon, 9 avenue Charles André, 69230 Saint-Genis Laval, France
[7] Georgia State University, PO Box 3969, Atlanta GA 30302-3969, USA
[8] CHARA Array, Mount Wilson Observatory, 91023 Mount Wilson CA, USA
[9] Observatório Nacional, Rua General José Cristino 77, 20921-400 São Cristovão, Rio de Janeiro, Brazil

Received 26 March 2010 / Accepted 10 June 2010

ABSTRACT

Context. BA-type supergiants are amongst the most optically-bright stars. They are observable in extragalactic environments, hence potential accurate distance indicators.
Aims. An extensive record of emission activity in the Hα line of the BA supergiants β Orionis (Rigel, B8Ia) and α Cygni (Deneb, A2Ia) is indicative of localized time-dependent mass ejections. However, little is known about the spatial distribution of these apparent structures. Here, we employ optical interferometry to study the Hα line-formation region in these stellar environments.
Methods. High spatial- (∼0.001″) and spectral- (R = 30 000) resolution observations of Hα were obtained with the visible recombiner VEGA installed on the CHARA interferometer, using the S1S2 array-baseline (34 m). Six independent observations were done on Deneb during the years 2008 and 2009, and two of Rigel in 2009. We analyze this dataset with the 1D non-LTE radiative-transfer code CMFGEN, and assess the impact of the wind on the visible and near-IR interferometric signatures, using both Balmer-line and continuum photons.
Results. We observe a visibility decrease in Hα for both Rigel and Deneb, suggesting that the line-formation region is extended (∼1.5–1.75 $R_\star$). We observe a significant visibility decrease for Deneb in the SiII 6371 Å line. We witness time variations in the differential phase for Deneb, implying an inhomogeneous and unsteady circumstellar environment, while no such variability is seen in differential visibilities. Radiative-transfer modeling of Deneb, with allowance for stellar-wind mass loss, accounts fairly well for the observed decrease in the Hα visibility. Based on the observed differential visibilities, we estimate that the mass-loss rate of Deneb has changed by less than 5%.

Key words. techniques: interferometric – stars: early-type – stars: mass-loss – stars: individual: HD 34085 – stars: individual: HD 197345 – circumstellar matter

1. Introduction

Supergiants of spectral types B and A (BA-type supergiants) are evolved massive stars of typical initial mass of 25–40 $M_\odot$ and high luminosity ($\gtrsim 10^5\,L_\odot$). Their luminosity and temperature place them among the visually brightest massive stars. Therefore, they are particularly interesting for extragalactic astronomy (Puls et al. 2008). Moreover, they represent attractive distance indicators by means of the identified wind-momentum-luminosity relationship (WMLR) (Kudritzki et al. 2008; Evans & Howarth 2003; Kudritzki et al. 1999). As a consequence, nearby BA supergiants have been analyzed with sophisticated radiative-transfer tools. Two subjects of intense scrutiny, both observationally and theoretically, have been Deneb (α Cygni, HD 197345, A2 Ia) and Rigel (β Orionis, HD 34085, B8Ia) (Schiller & Przybilla 2008; Aufdenberg et al. 2006b, 2002, for Deneb).

Intensive spectroscopic monitoring of the activity of wind-forming lines, such as Hα, suggests that the stellar-wind variability of luminous hot stars is associated with localized and co-rotating surface structures. The pioneering work of Lucy (1976) based on a period analysis of radial-velocity curves of Deneb obtained in 1931/32 by Paddock (1935) revealed the simultaneous excitation of multiple non-radial pulsations (NRPs). This effort was followed by the extended optical HEROS campaigns (Kaufer 1998), monitoring for ∼100 consecutive nights late B-type/A-type supergiants (Kaufer et al. 1997, 1996a,b) and early B-type hypergiants (Rivinius et al. 1997). Attempts to associate this activity with large-scale surface magnetic fields have so far been

⋆ Based on observations made with the CHARA array.

unsuccessful (Schnerr et al. 2008; Verdugo et al. 2003; Henrichs et al. 2003; Bychkov et al. 2003). However, the appearance of thin surface convection zones at the supergiant stage may favor the formation and emergence of magnetic fields (Cantiello et al. 2009), and may also have a significant impact on potential NRPs.

BA-type supergiants such as Rigel (B8 Ia) and Deneb (A2 Ia) exhibit observational evidence of the random and pseudo-cyclic activity of the stellar wind. A pulsation-driving mechanism has often been proposed, although the associated micro-variability is observed for a wide range of luminosity and $\log T_{\rm eff}$. Gautschy (1992) argued for the presence of strange modes. Gautschy (2009) tentatively proposed that Deneb's micro-variability is caused by a thin convection zone efficiently trapping the non-radial oscillations, and significant progress has been made in determining the mechanism leading to mass ejection (Cranmer 2009). The collective effect of multiple NRPs was also proposed as a promising means of explaining the large value of the macro-turbulence parameter; NRPs also represent an attractive mechanism for the formation of Be-star disks (Aerts et al. 2009; Neiner et al. 2009).

Based on intensive monitoring of spectroscopic lines, many observational campaigns have attempted to discriminate between these models. Monitoring of Deneb and Rigel is still ongoing (Danezis et al. 2009; Morrison et al. 2008; Rzaev 2008; Markova et al. 2008; Markova & Puls 2008; Morel et al. 2004; Rivinius et al. 1997; Kaufer et al. 1996b, for a non-exhaustive list).

The uniform-disk (UD) angular diameters of Deneb and Rigel are 2.4 mas and 2.7 mas, respectively (Aufdenberg et al. 2008; Mozurkewich et al. 2003), making them good targets for accurate long-baseline optical interferometry. An extensive study of Deneb was performed by Aufdenberg et al. (2002), using different radiative-transfer models (with allowance for the presence of a wind), and constraints from optical interferometry data. Deneb's wind should enhance the limb darkening relative to hydrostatic models that neglect it. However, this can only be constrained observationally by using long baselines in the near-IR (longer than 250 m) or by observing in the visible, thus relaxing the constraints on the baselines by a factor of about 3–4. The Hα line is particularly interesting in that context. Its large opacity makes it very sensitive to changes at the stellar surface and above, in particular through modulations in stellar-wind properties. Its extended line-formation region is therefore more easily resolved than the deeper-forming continuum. Dessart & Chesneau (2002) investigated the possibility of monitoring the mass-loss activity in wind-forming lines by means of optical interferometers equipped with spectral devices of sufficient dispersion.

BA supergiants rotate slowly ($v \sin i$ of about 25–40 km s^{-1}), at least relative to their terminal wind-velocity of ~200–400 km s^{-1}. Spectrally resolving the Doppler-broadened Balmer lines thus requires a resolving power as high as $R = 10\,000$. At optical wavelengths, the most conspicuous indicator of mass-loss in early-type supergiants is Hα, which exhibits the distinctive P-Cygni profile morphology and has often been a crucial estimator of the mass-loss rate in spite of its documented variability. While Aufdenberg et al. (2002) was successful in reproducing many observables obtained for Deneb, the modeling of the Hα line proved difficult. The most significant and persistent discrepancy between the synthetic and observed profiles has been the depth of the absorption component, which is significantly weaker in the observed spectrum (residual intensity ~0.6). Furthermore, while the velocity of the absorption component minimum is quite variable, it is rarely, if ever, shifted blueward by more than ~50 km s^{-1}, which is ~20% of the terminal velocity. Schiller & Przybilla (2008) used a different strategy, using the Hα profile as a reference for a detailed modeling of the wind characteristics, and reached a more satisfactory solution. Nevertheless, they also reported some remaining discrepancies in matching the Hα absorption, and proposed additional effects that may need to be considered in the modeling, such as wind structure or the influence of a weak magnetic field.

Table 1. VEGA/CHARA observing logs.

Date	Time	SCI/CAL	Projected baseline	
			Length [m]	PA [°]
2008.07.28	06:04	Deneb	33.4	6.2
2008.07.28	09:01	Deneb	32.9	–18.8
2008.07.28	10:51	Deneb	26.2	–46.7
2008.07.30	05:20	Deneb	33.3	10.3
2008.07.30	07:42	Deneb	32.3	–9.9
2008.07.30	11:32	Deneb	30.1	–37.6
2009.07.27[b]	07:51	CAL1[a]	31.8	–19
2009.07.27[b]	08:11	Deneb	33.3	–11.1
2009.07.27[b]	08:28	CAL1[a]	31.4	–23
2009.08.26	06:51	CAL1[a]	31.1	–26.8
2009.08.26	07:06	Deneb	33.0	–18.5
2009.08.26	07:25	CAL1[a]	30.5	–31.0
2009.10.01	03:56	Deneb	33.2	–14.3
2009.10.01	04:34	CAL1[a]	33.2	–14.3
2009.10.01	05:56	Deneb	32.2	–27.3
2009.10.01	11:35	Rigel	25.3	–6.5
2009.10.25[b]	02:21	Deneb	32.3	–26.2
2009.11.17	01:35	Deneb	32.8	–20.4
2009.11.17	09:48	Rigel	27.1	–20.5

Notes. [(a)] CAL1: HD 184006, A5V, $V = 3.7$, estimated diameter 0.6 ± 0.05mas from SearchCal@JMMC. [(b)] Observations performed remotely from France.

The VEGA recombiner of the CHARA array is a recently commissioned facility that provides spectrally dispersed interferometric observables, with a spectral resolution reaching $R = 30\,000$, and a spatial resolution of less than one *mas*. The instrument recombines currently the light from two telescopes, but 3–4 telescope recombination modes are foreseen in a near future. The Hα line of bright, slow rotators such as Deneb or Rigel can be isolated from the continuum, and the spatial properties of the line-forming region can thus be studied with unprecedented resolution. Using the smallest baseline of the CHARA array (baseline of 34 m), we conducted a pioneering temporal monitoring of Deneb uncovering a high level of activity in the Hα line-forming region. Rigel was also observed a few times.

The paper is structured as follows. In Sect. 2 we present the optical interferometry data and their reduction, in addition to complementary spectra obtained by amateur astronomers. We then review in Sect. 3.1 the previous interferometric measurements aiming to more tightly constrain the diameter of Rigel and Deneb. We then apply this extensive record of measurements in the visible and near-IR continuum to interpret semi-quantitatively the spectrally-dispersed measurements in Sect. 3.2, and to elaborate a radiative-transfer model of the stars in Sect. 4.

2. Observations and data processing

2.1. VEGA observations

Deneb and Rigel were observed with the Visible spEctroGraph And Polarimeter (VEGA instrument, Mourard et al. 2009) integrated within the CHARA array at Mount Wilson Observatory (California, USA, ten Brummelaar et al. 2005). Deneb observations were carried out at regular intervals between July 2008 and November 2009. Rigel observations were performed in October-November 2009. The VEGA control system can be handled from France remotely. A detailed description of this control system is presented in Clausse (2008).

The red detector was centered around 656 nm, and we made use of the high-resolution mode ($R = 30\,000$). For each observation, VEGA recombined the S1 and S2 telescopes forming the S1S2 baseline. This is the smallest baseline of the array, for which the extended Hα emission is not over-resolved. The S1S2 baseline is almost aligned north-south and the projection of the baseline onto the sky does not vary much during the night. This is considered an advantage in the context of our observations, which are designed to detect the time variability of the Hα line-forming region. Details of the observations can be found in Table 2. On several occasions, more than one acquisition of Deneb was performed during the night, providing interesting, albeit limited information about the spatial asymmetry of the source. Since our goal was to investigate the spectral and spatial properties of the Hα line relative to the continuum, emphasis was not placed on obtaining very precise calibration of the absolute visibilities. The angular diameters of Rigel and Deneb are well known (see Sect. 3.1), so we relied on the published values to scale the continuum absolute visibilities. Moreover, it is difficult to find a suitable bright calibrator when observing at high spectral resolution, which is not well-suited to an accurate determination of the absolute visibility which implies a large continuum window. Improving upon the current determination of the angular diameter in the visible would require a dedicated observing strategy using the medium-resolution mode, larger baselines coupled with a fringe tracking performed in the near-IR. This possibility is foreseen in the future. Therefore, calibrator observations were not performed systematically, but only to ensure that the instrument was behaving well.

The data reduction method is fully described in Mourard et al. (2009) and we only summarize it shortly here. The spectra are extracted using a classical scheme, of collapsing the 2D flux in one spectrum, wavelength calibration using a Th-Ar lamp, and normalization of the continuum by polynomial fitting. We note that the photon-counting cameras saturate when the rate of photons is too high locally. Because of the brightness of the sources, neutral density filters of 0.6 to 1 mag had to be applied, depending on the atmospheric conditions and the spread of the speckle images on the slit. Spectra with a signal-to-noise ratio (SNR) of 300–400 were routinely obtained, although clear signs of saturation were found in a few of them. After careful testing, we checked that the saturation had only a very limited effect on the interferometric measurements. When the quality of the spectra was such that telluric lines are observable, these are used to refine the wavelength calibration, although most of the time the VEGA spectral calibration was checked against the reference spectra obtained by amateur astronomers. A series of spectra for Deneb is shown in Fig. 1.

The raw squared visibilities (V^2) were estimated by computing the ratio of the high frequency energy to the low frequency energy of the averaged spectral density. The same treatment was applied to the calibrators, whose angular diameter was computed using the software SearchCal[1] (Bonneau et al. 2006). The expected absolute visibilities of VEGA in the continuum from the short baselines do not provide strong constraints on the angular diameter and a calibrator was not systematically observed. When such an observation is available, we carefully checked that the observed visibilities were compatible with the expected ones. A

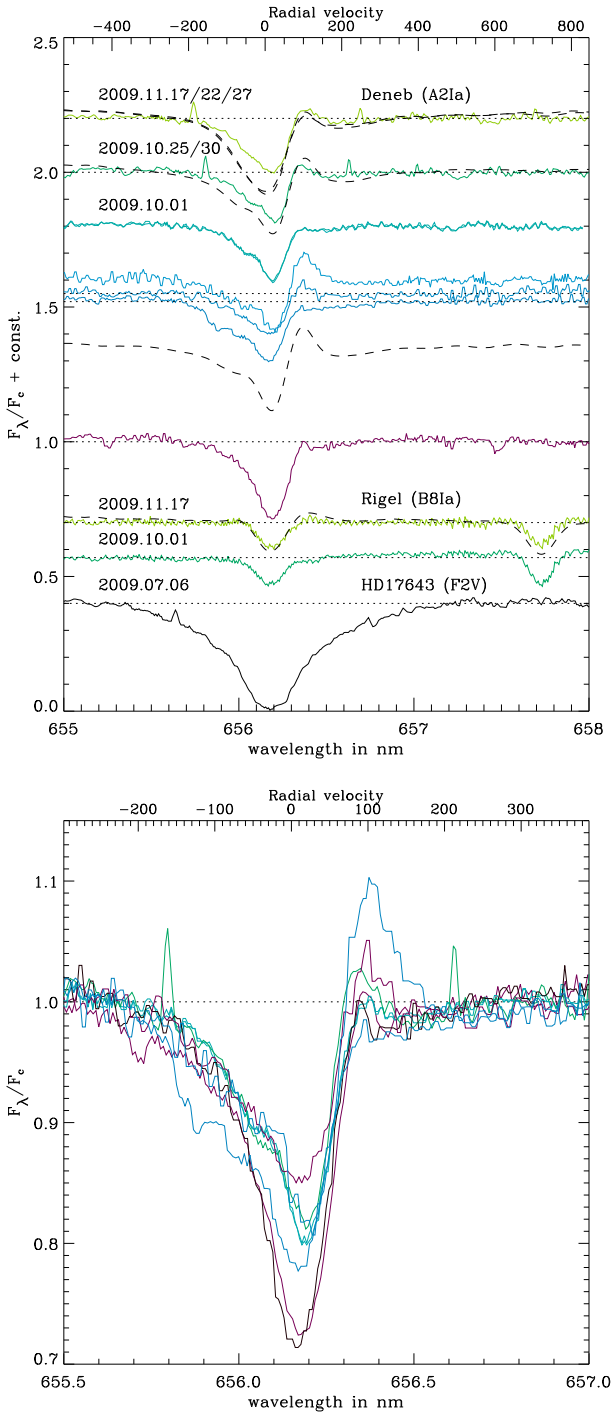

Fig. 1. *Top*: montage of Hα observations at various epochs for Deneb and Rigel. We also include one observation of the calibrator (HD 17643). The dashed lines indicate the spectra recorded by amateur astronomers. *Bottom*: normalized multi-epoch Hα observations of Deneb. The color coding is the same as that used in *the top panel*.

[1] http://www.jmmc.fr/searchcal/

Table 2. VEGA/CHARA V^2 measurements performed on 2009.07.27 and 2009.08.26.

Date	Wavelength [nm]	Baseline [m]	V^2	V^2 error
2009.07.27	654	32.97	0.421	0.019
2009.07.27	657	32.97	0.444	0.024
2009.07.27	630	32.97	0.376	0.016
2009.08.26	654	33.19	0.418	0.051

contemporary measurement obtained with the medium resolution mode is presented in Mourard et al. (2009).

The information in a line was extracted differentially by comparing the properties of the fringe between a reference channel centered on the continuum of the source, and a sliding science narrow channel, using the so-called cross-spectrum method (Berio et al. 1999). The absolute orientation of the differential phase was established by considering the change in the spectral slope of the dispersed fringes (Koechlin et al. 1996) when changing the delay line position. Thus a *positive* value corresponds to a photocenter displacement along the S1S2 projected baseline *in the south direction*.

The width of the science channel was 0.02 nm in good atmospheric conditions, and degraded to 0.08 nm in poor weather conditions. The rms of the spectrally dispersed visibility in the 654–655 nm continuum ranges from 3–4% at visibility 1 in the highest quality nights (2008/07/28, 2008/07/30, 2009/10/01) to about 7–8% in medium nights (2009.07.27, 2009.08.26) and more than 10% in poor nights (2009/11/17). The rms of the differential phases follows the same trend ranging from 1–2° in good conditions, to 3–4° in medium conditions, and 5–6° in poor conditions. Figures 2, 3 illustrate the best observations of Deneb secured in 2008. A Gaussian fit was applied to the differential visibilities and phase to retrieve accurate information about the spectral *FWHM* and position of the interferometric signal. The spectral location of the differential visibility and differential phase dips are stable at a level of 0.005 nm (~3 km s^{-1}). Information from the blue camera was also used, as some important lines, e.g. SiII 6343–6371 Å can be investigated (see Fig. 3 and Sect. 3.3).

2.2. Spectroscopy from amateur astronomers

Several Hα spectra were obtained during the same period with the 0.28 m amateur telescope (Celestron 11) located in Castanet-Tolosan (France) equipped with the eShel spectrograph and a QSI532 CCD camera (CCD KAF3200ME). These spectra were used in this study as an indication of the emission level and variability of the stars. The typical resolution of these spectra is ~11 000.

The reduction of these data was performed using the standard echelle pipeline (Reshel software V1.11). H2O telluric lines are removed by means of division by a synthetic H2O spectrum using Vspec software – the telluric-line list was taken from GEISA database (LMD/CNRS). We corrected for the diurnal and annual earth velocity are corrected for (spectral wavelengths are given in an heliocentric reference for a standard atmosphere). Systematic differences were found in the VEGA/CHARA and amateur continuum correction producing the differences seen in Fig. 1 between the solid (VEGA) and dashed lines (eShel).

3. Results

3.1. The diameters of Deneb and Rigel

For the most accurate estimates to date of the diameters of Rigel and Deneb, we refer to Aufdenberg et al. (2008, 2006a), in which CHARA/FLUOR observations in the K band with baselines reaching 300 m are described. These observations infer a UD angular diameter of 2.76 ± 0.01 mas, and 2.363 ± 0.002 mas, for Rigel and Deneb, respectively. To first order, no significant change in these diameters inferred from the visible or the near-IR is expected, the wind being too tenuous to shift the continuum-formation region (see Sect. 4). This value of the Deneb UD angular diameter agrees with the optical measurements of Mozurkewich et al. (2003) obtained with the MarkIII interferometer using multiple observations with baselines ranging from 3 m to 28 m with 2.34 ± 0.05 mas at 0.8 μm, 2.26 ± 0.06 mas at 0.55 μm, and 2.25 ± 0.05 mas at 0.41 μm. The few V^2 measurements secured from the present observations with a very limited spatial frequency range agree with the MarkIII measurements. We estimated the uniform disk diameter of Deneb using only the red camera to be 2.31 ± 0.04 mas at 0.65 μm, and using both cameras found the diameter to be 2.34 ± 0.03 mas. Only the best observations could be used, as the visual magnitude of the calibrator (V = 3.7) was too faint to often obtain a reliable estimate of the absolute visibility, even using the broadest possible spectral band (i.e. 5 nm).

3.2. The Hα line-formation region

The Hα line is one of the most optically thick of all lines seen in the optical and near-IR spectra of hot stars, hence represents an excellent tracer of their winds. This line has mostly been observed by means of spectroscopy at various spectral resolution, and in some dedicated campaigns with a very intensive time coverage aimed at recovering the time variability of the line-forming region. We refer to Rzaev (2008) and Morrison et al. (2008) for the latest reports on Deneb and Rigel. This conspicuous line-profile variability suggests that the wind itself, where the Hα line forms, is variable in its properties. For example, variations may take place in the ionization, the morphology, or the density structure of the wind. The significant changes in the line-profile shape with time indicates that the Hα line-formation region is asymmetric, and that this asymmetry changes with time.

The Hα line observed in Deneb exhibited evidence of some activity during the 2008–2009 observations, but not of any dramatic change in mass-loss rate. The Rigel spectra were also obtained during what appears to have been quiet periods and differ from the "typical" spectrum shown in Fig. 1 of Morrison et al. (2008). As can be seen here in Fig. 1, the Hα line is as deep as the carbon CII lines at 657.8 and 658.3 nm in Rigel. This is not an unusual state, as Hα often appears in pure absorption and to be symmetric about the line center (in the rest-frame) about 20% of the time (using Morrison et al. (2008) statistics).

Both the Deneb and Rigel dispersed visibilities exhibit a profound dip in the Hα line, suggesting that the line forms over an extended region above the continuum. These dips are symmetric about the line center (in the rest-frame) in both objects. The *FWHM* of the visibility dip was estimated by performing a Gaussian fit to data of the high quality nights in 2008. These measurements yield a *FWHM* of 0.215 ± 0.007 nm, i.e. 98 ± 3 km s^{-1} for Deneb (Fig. 2). By comparison, the visibility signal is narrower for Rigel, with a *FWHM* of 70 ± 5 km s^{-1}. One can estimate the visibility in the line by using a continuum

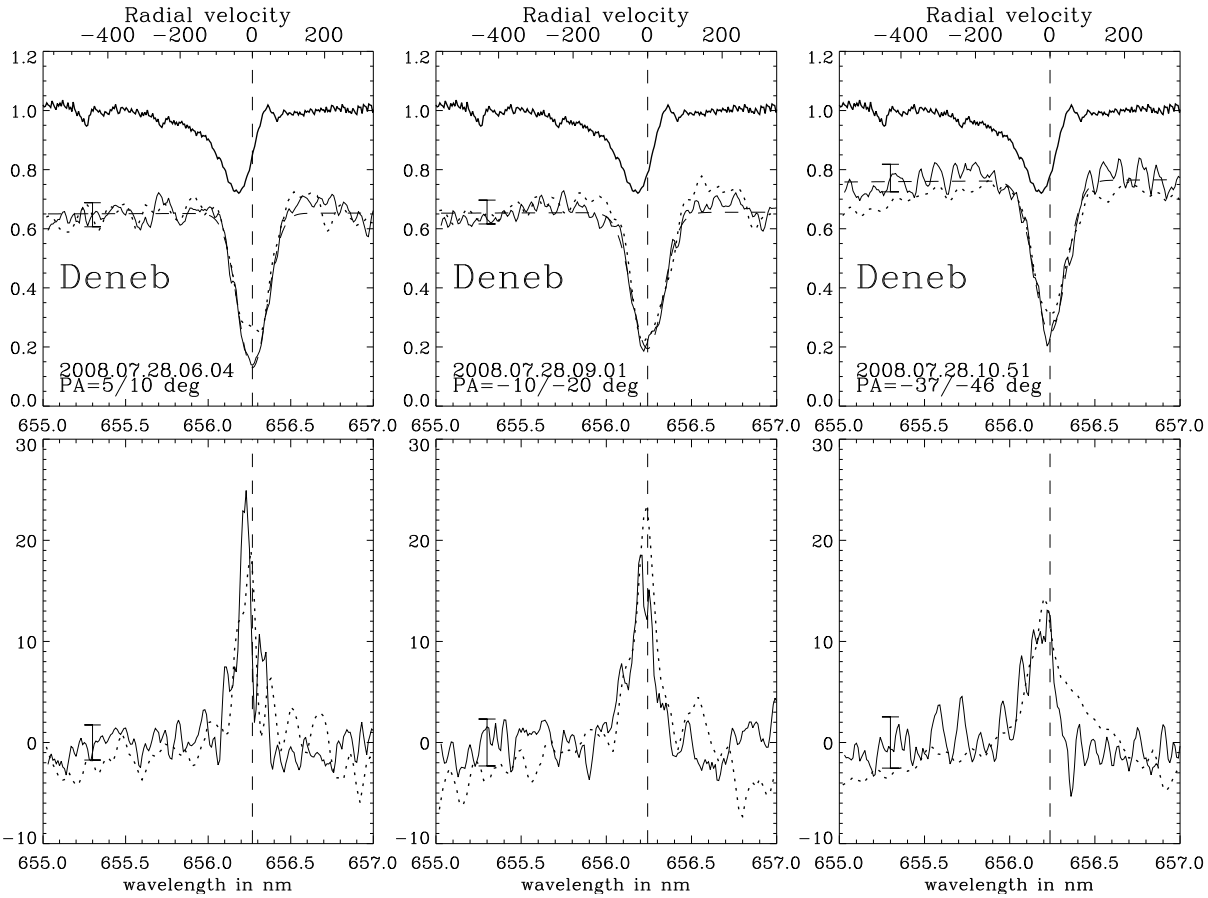

Fig. 2. *Top row*: normalized flux (upper curve) and dispersed visibility (lower curve; spectral band 0.02 nm) for the Hα observations of Deneb obtained on 2008.07.28 (solid line) and on 2008.07.30 (dotted line). The resolution is $R = 30\,000$. *Bottom*: same as top row, but now for the differential phase. A strong signal changing with baseline direction is observed, indicating that there was a significant asymmetry in the line-forming region at this time.

derived from published values of the angular diameter. The corresponding UD estimates for the highest extension of the Hα line-forming regions are 4.1 ± 0.2 mas and 4.2 ± 0.2 mas for Deneb and Rigel, representing 1.75 and 1.5 $R_\star$, respectively.

The differential phases are a direct indication of the position of the Hα line-forming regions at different radial velocities, by comparison to the continuum considered as the reference of phase. For the 2008 data, the Gaussian fits provide *FWHM*s that increase from the baselines oriented near +10° to –40° from 61 ± 2 km s^{-1} to 84 ± 4 km s^{-1}. Sub-structures are also detected, with the highest peak near the zero velocity, and two satellites at about 40 km s^{-1}. The peak level reached by the differential phases follows a trend from a large photo-center shift at PA close to 5–10° that decreases toward −30–50°.

The differential phases recorded for Deneb between 2008 and 2009 are shown in Fig. 5. Dramatic changes are observed with periods of large phase signal alternating with periods containing no detectable signal.

The "calm" periods may potentially provide important information about the rotation of the star. This characteristic signal can be observed in the rotating circumstellar environment of Be-star disks (see Delaa et al. in preparation; Berio et al. 1999; Vakili et al. 1998; Stee 1996), and also directly on the photosphere of a rotating star (Le Bouquin et al. 2009). Approaching and receding regions of a rotating star experience different Doppler shifts and are thus spectrally separated. In the sky, the natural consequence is that the line-absorbing regions are seen by the interferometer at one or the other side of the continuum, generating the well-known S-shape signal in the differential phases. This signal might have been detected in Rigel data of the 2009-10-01 (see Fig. 4). The rms of the phase of these data is 7.7°, and the maximum and minimum of the signal are at 26° and –17°, respectively, at the blue and red sides at ∼15 km s^{-1} from line center. The signal is kept at a similar level when extracted with a double binning of 0.04 nm, and the phase rms is decreased to 5.6°. This is on the order of the estimated $v \sin i$ of the source of about 36 km s^{-1}. We were unable to detect a similar signal for Deneb probably because of the limited spectral resolution, insufficient to resolve its low estimated $v \sin i$ of 20 km s^{-1}. As the signal is anti-symmetric, it cancels out if the spectral resolution is too low. One must also keep in mind that the quality of the data fluctuated and that the binning could not be kept identical at all epochs. It is not impossible that weak signals are blurred (such a signal might be visible the 2009/11/17; Fig. 5). Given the large extension and the activity observed in the differential phases in Hα, this line is probably not ideally suited to inferring the rotation of the star.

To first order, and for marginally resolved sources, the differential phases can be considered to linearly depend on the photo-center position of the emitting source. This is no longer the case when the source is significantly resolved as in our case, but we consider this as a rough estimate. Assuming that

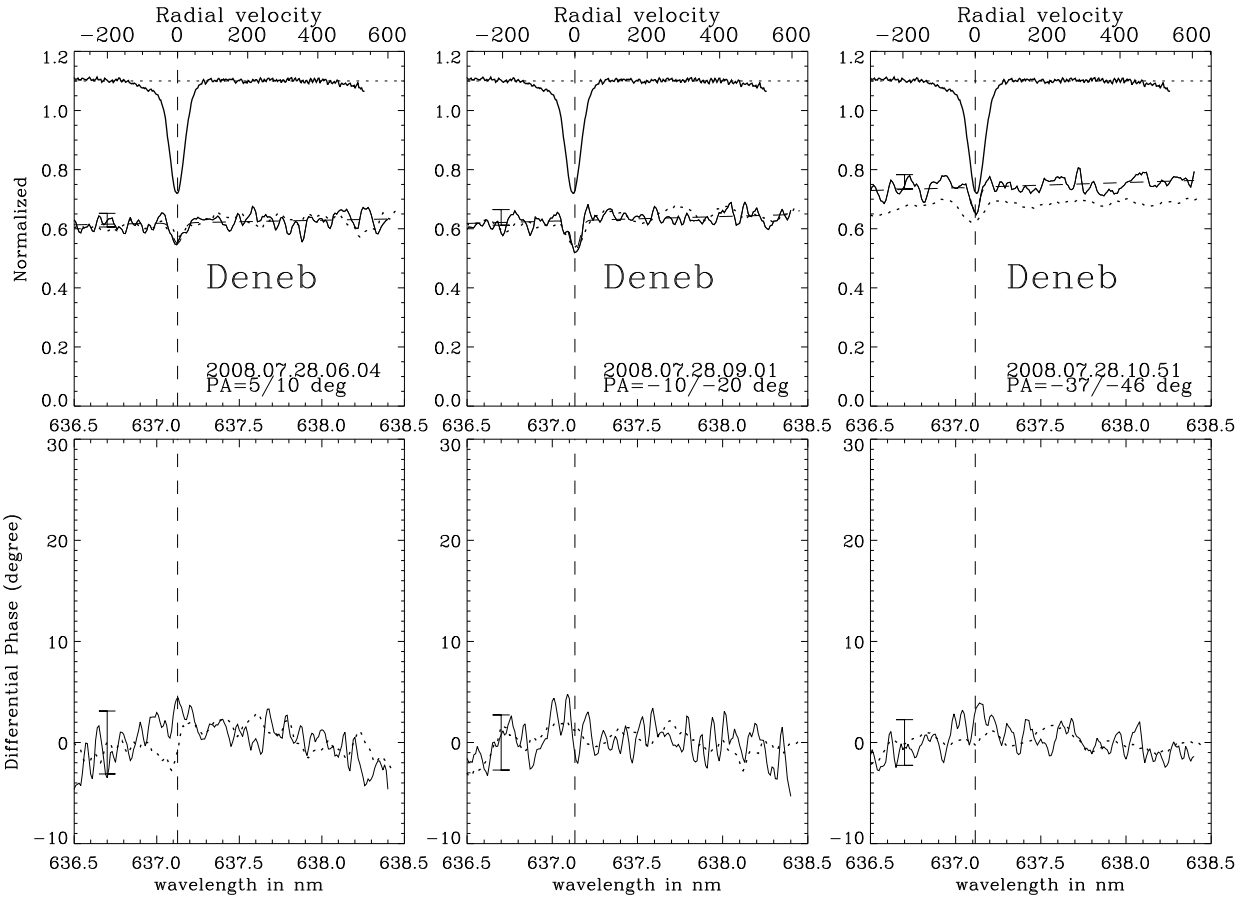

Fig. 3. Same as Fig. 2, but now showing Deneb observations obtained with the blue camera, whose spectral range covers the SiII 6371 line. For a clearer comparison, the ordinate ranges are kept identical. The SiII 6371 line is seen as a strong absorption (the continuum level of the spectrum is offset by 0.1 for clarity), marginally resolved by VEGA/CHARA. However, no phase signal is observed.

the line emission represent a fraction $f_{\rm ratio}$ of typically 50% of the light in the Hα line core, the following relation is used $p = -(\phi/360)(\lambda/B)(1/f_{\rm ratio})$. We find that the astrometric shifts induced by the inhomogeneous Hα emission reach 0.5 mas (0.2 $R_\star$), but are lower than 0.3 mas most of the time. The event observed in 2008 is remarkable as the full line appeared to be off-center relative to the continuum. A similar event was observed on 2009/10/01 to have an opposite direction.

3.3. The Si II 6347–6371 Å line-formation regions

The SiII 6371 line was observed simultaneously with the Hα line in the blue camera (Fig. 3) in 2008. The line profile shows a pure absorption, but is slightly asymmetric with an extended blue wing due to extended absorption in the wind regions. The VEGA/CHARA observations of Deneb obtained in 2008 indicate that the line-formation region of the SiII 6371 line is more extended than the continuum forming region, with differential-visibility dips of 10%, 19%, and 15% for baselines in the range [5°:10°], [–10°:–20°], and [–35°:–50°]. The rms of the dispersed visibilities is 5%. The line *FWHM* estimated from Gaussian fitting is 55 ± 3 km s^{-1} and the *FWHM* of the visibility dip is narrower with a *FWHM* decreasing from 33 ± 4 km s^{-1} to 24 ± 4 km s^{-1} for PA from [5°:10°] to [–35°:–50°], respectively. One can roughly estimate the extension of the line-forming region using the minimum of the visibility and UD approximation to be 2.6 mas, 2.7 and 2.75 mas using the value of 2.34 mas from NPOI as the diameter at 630 nm. One may speculate whether this trend in the visibilities is permanent or a transient event closely related to the asymmetries inferred from the differential phases in the Hα line. Because of a spectrograph realignment carried out in 2009, the SiII 6371 line was not any longer observable with the blue camera in 2009, but the SiII 6347 was well-centered and could be analyzed. No such signal was observed at anytime.

Despite the large depth of the silicon lines, no differential-phase signal was detected above an rms of $\lesssim 2°$. This means that the imprint of the rotation of the star on the SiII line-formation region is not detected in the data, probably because of insufficient spectral resolution. Strong SiII lines were also observed in Rigel's spectrum, but neither differential visibility nor any phase signal was detected. The SNR of the data is poorer than the Deneb observations, with an rms in the dispersed visibilities and phases of 10%.

4. Comparison with radiative transfer models

The BA supergiants, especially nearby ones, have been extensively studied with sophisticated radiative-transfer codes. It is not in the scope of this paper to determine more reliably the fundamental parameters of Deneb or Rigel. However, we wish to investigate several important issues related to the putative effects of the wind on the interferometric observables. Deneb has been observed by several northern-hemisphere interferometers

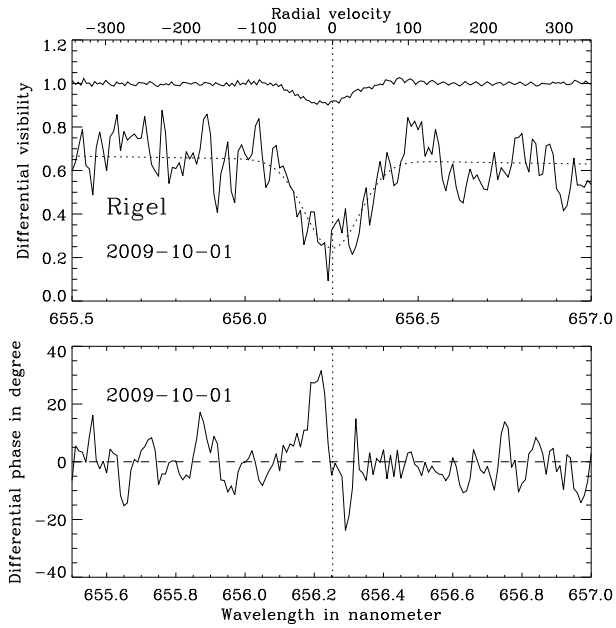

Fig. 4. *Top*: Hα observations of Rigel on 2009.10.01 (upper curve), and the corresponding differential visibility, scaled to the expected absolute level of the continuum (lower curve). *Bottom:* Differential phase curve exhibiting a clear S-shape signal, indicative of rotating circumstellar material. A vertical dotted line is shown in both panels to indicate the location of the Hα rest-wavelength determined by a Gaussian fitting of the visibility curve.

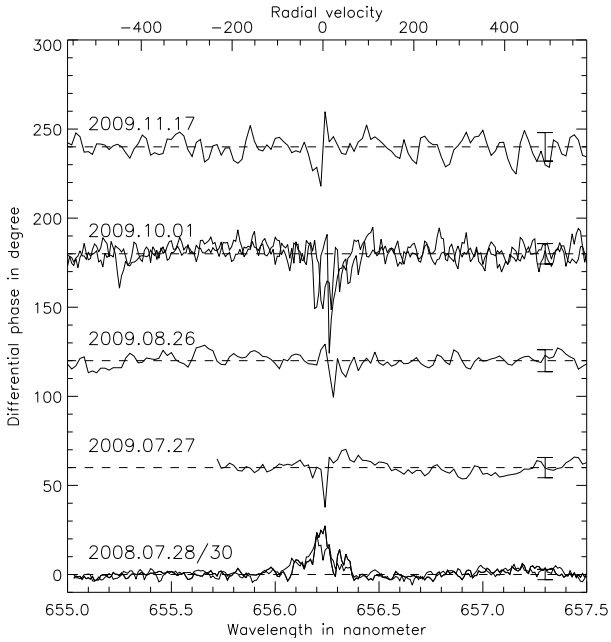

Fig. 5. Time evolution of the differential phases of Deneb. The strong phase signal observed in 2008 is indicative of a very asymmetric environment, off-centerd from the continuum source. No clear S-shape signal is observed, in agreement with the low $v \sin i$ of Deneb of $\sim$20 km s^{-1}, unresolved by the instrument.

in both the visible and the near-IR. Rigel is currently monitored with VEGA/CHARA in the northern hemisphere, as well as in the southern hemisphere with the VLTI. Hence, in this study, we used the stellar parameters obtained by Przybilla et al. (2006) and Schiller & Przybilla (2008) for Rigel and Deneb, respectively. After developing a convergent model for a reference mass-loss rate value at which Hα is predicted in absorption, we then increased the mass-loss rate (keeping the other stellar parameters fixed) until the Hα line exhibited a well-developed P-Cygni profile. In this way, we explored the followings questions:

- to what extent the angular diameter inferred from optical and near-IR continua is sensitive to changes in mass-loss rates?
- are the Hα, Paβ, and Brγ line-formation regions reproduced by radiative-transfer simulations accounting for a wind? These lines form in different parts of the wind and can thus be used simultaneously to constrain its properties.

In this paper, we focus on the Hα line because it can be observed with VEGA/CHARA. A similar study for Paβ and Brγ line-formation regions is postponed to another paper in preparation.

4.1. Numerical simulations

Our radiative-transfer calculations were carried out with the line-blanketed non-LTE model-atmosphere code CMFGEN (Hillier & Miller 1998; Dessart & Hillier 2005), which solves the radiation-transfer equation for expanding media in the comoving frame, assuming spherical symmetry and steady-state, and under the constraints set by the radiative-equilibrium and statistical-equilibrium equations. It treats line and continuum processes, and regions of both small and high velocities (relative to the thermal velocity of ions and electrons). Hence, it can solve the radiative-transfer problem for both O stars, in which the formation regions of the lines and continuum extend from the hydrostatic layers out to the supersonic regions of the wind, and Wolf-Rayet stars, in which lines and continuum both originate in regions of the wind that may have reached half its asymptotic velocity.

We used the stellar parameters inferred by Schiller & Przybilla (2008) for Deneb, and by Przybilla et al. (2006) and Markova et al. (2008) for Rigel. The MgII resonance lines suggest terminal wind speeds of $\sim$240 km s^{-1} for Deneb (Schiller & Przybilla 2008) and $\sim$230 km s^{-1} for Rigel (Kaufer et al. 1996b). Their projected rotational velocities are low, i.e. 20 ± 2 km s^{-1} and 36 ± 9 km s^{-1} respectively.

Even for sources as "close" as Deneb and Rigel, the distance estimates remain quite inaccurate. Schiller & Przybilla (2008) derived a luminosity of $1.96 \times 10^5\, L_\odot$ for Deneb, using a distance of 802 ± 66 pc (assuming that Deneb is a member of the Cyg OB7 association), while the one derived from Hipparcos (van Leeuwen 2007) is significantly smaller (i.e., 432 ± 61 pc), which infers a luminosity estimate of $5.5 \pm 1 \times 10^4\, L_\odot$. This reassessment directly scales down by almost a factor two the linear scales of the size parameters. Furthermore, recalling that the mass-loss rate scales with the luminosity, this should imply a weaker steady-state wind mass loss for Deneb. The corresponding uncertainties are considerably lower for Rigel, which is much closer than Deneb.

By adopting values these parameters from previous works, we find that the synthetic spectra computed by CMFGEN agree favorably with the observations. We thus adopt these stellar parameters and vary the mass-loss rate value to assess the impact on the spectrum and in particular Hα and SiII 6347–6371.4 Å. In practice, we explore the effect of a wind mass-loss rate of 1.55, 3.1, 6.2, and $12.4 \times 10^{-7}\, M_\odot$ yr^{-1} for Deneb, and values of 1, 2, 4, and $8 \times 10^{-8}\, M_\odot$ yr^{-1} for Rigel. A typical effect that appears in theoretical models is illustrated in the bottom panels

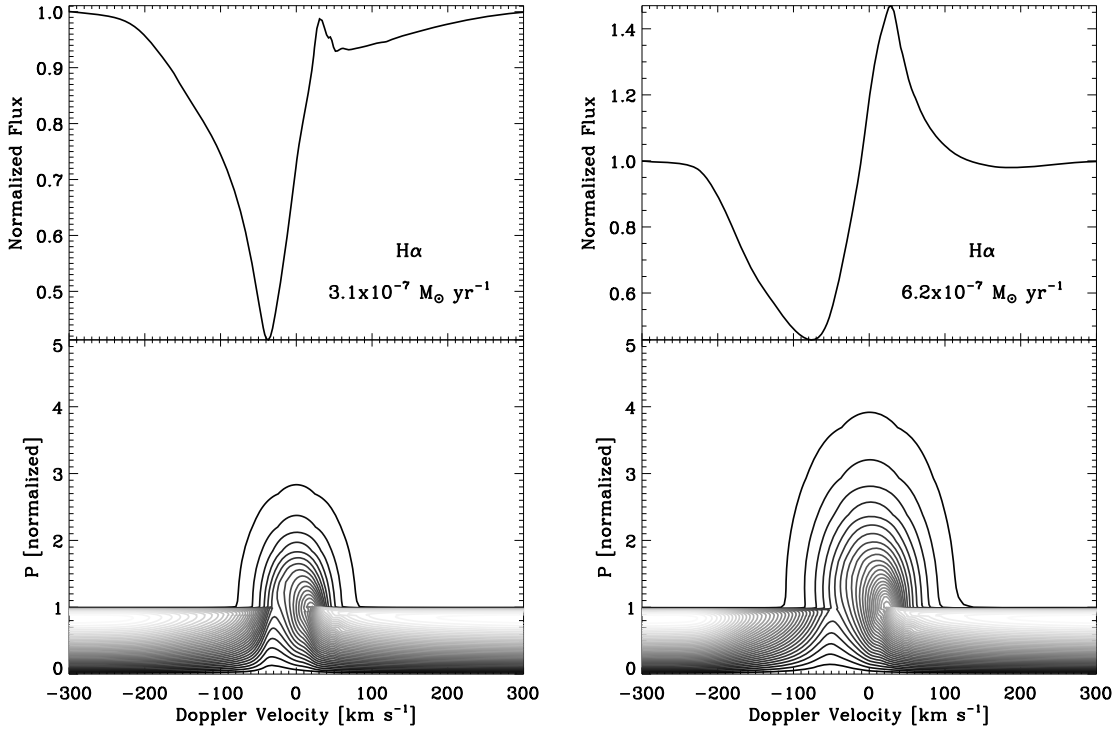

Fig. 6. *Left*: In *the bottom panel*, we show a contour plot of the quantity $P \times I(P)$ as a function of Doppler velocity and impact parameter P for Hα, computed with CMFGEN using the stellar parameters of Deneb and a mass-loss rate value of $3.1 \times 10^{-7}\ M_{\odot}\ \mathrm{yr}^{-1}$, corresponding to the best-fit model. This figure illustrates the distribution of intensity with impact parameter, and in particular serves to infer the regions that contribute significant flux to the line, and hence the spatial extent of the Hα line-formation region. In *the top panel*, we show the corresponding normalized synthetic flux in Hα. *Right*: same as left, but now for a mass-loss rate value of $6.2 \times 10^{-7}\ M_{\odot}\ \mathrm{yr}^{-1}$. Notice the sizable change in profile morphology, echoing the change in the extent of the line-formation region.

of Fig. 6, where we show the distribution of the emergent intensity I (scaled by the impact parameter p), as a function of Doppler velocity and p. This type of illustration was introduced by Dessart & Hillier (2005) to study line formation in hydrogen-rich core-collapse supernova ejecta. Here, it provides a measure of the extent of the line-formation region of Hα relative to the neighboring continuum and the sites where most of the emergent photons originate. Comparing the left and right panels suggests that a variation by a factor of two in the mass-loss rate value leads to sizable changes in the extent of the line-formation region, and correspondingly, large changes in the observed line profile. While spectroscopy is sensitive to the latter, interferometry is sensitive to the former. Below, we describe the interferometric signals associated with these intensity maps computed with CMFGEN and produced using the stellar parameters suitable for Rigel or Deneb, and various mass-loss rates tuned to match observations. This is illustrated in Fig. 7 in the case of Deneb and Rigel, using two different mass-loss rates. The visibility curves for various spectral channels in the vicinity of Hα are plotted as a function of the spatial frequency. The differential visibilities observed by VEGA are generating by plotting the different value for a given projected baseline (between 27 m and 33 m).

4.2. Visible and near-IR continuum forming regions

In Fig. 10, we show a zoom of the 0.6 μm and 2.2 μm squared-visibility curves of Deneb in the second lobe with the various mass-loss rate values used in this paper. The visible continuum appears to be far more sensitive to such changes than the near-IR continuum. We note that these visibility curves are computed for a spectral resolution of 30 000, and cannot be directly compared with the broadband measurements of FLUOR/CHARA over the full K'-band (Aufdenberg et al. 2008).

Doubling the mass-loss rate from 3.1 to $6.2 \times 10^{-7}\ M_{\odot}\ \mathrm{yr}^{-1}$ does not significantly alter the optical thickness of the wind. The angular diameter of the star in the continuum near Hα determined by a UD fitting of the visibility curve does not therefore change by more than 2%. However, we note that the second lobe is significantly affected. This conclusion is also true in the near-IR. All models also show that the near-IR UD angular diameter is systematically larger than the visible one by ~2.5–3%, due to the increasing continuum opacity with wavelength (free-free and bound-free processes). The near-IR models were scaled to match the accurate CHARA/FLUOR value of 2.363 mas, and this implies that the expected UD diameter in the Hα overlapping continuum is $\sim 2.31 \pm 0.02$ mas. This expectation agrees with the NPOI measurements of 2.34 ± 0.05 mas at 0.8 μm and 2.26 ± 0.06 mas at 0.55 μm.

For Rigel, the difference between the near-IR UD angular diameter and its visible counterpart is increased slightly to reach ~3.0–3.5%. Using the FLUOR/CHARA measurement of 2.758 mas as reference, this would imply a diameter of about 2.64 mas in the visible. In the near-IR, some instruments such as FLUOR/CHARA have an accuracy often better than 1%

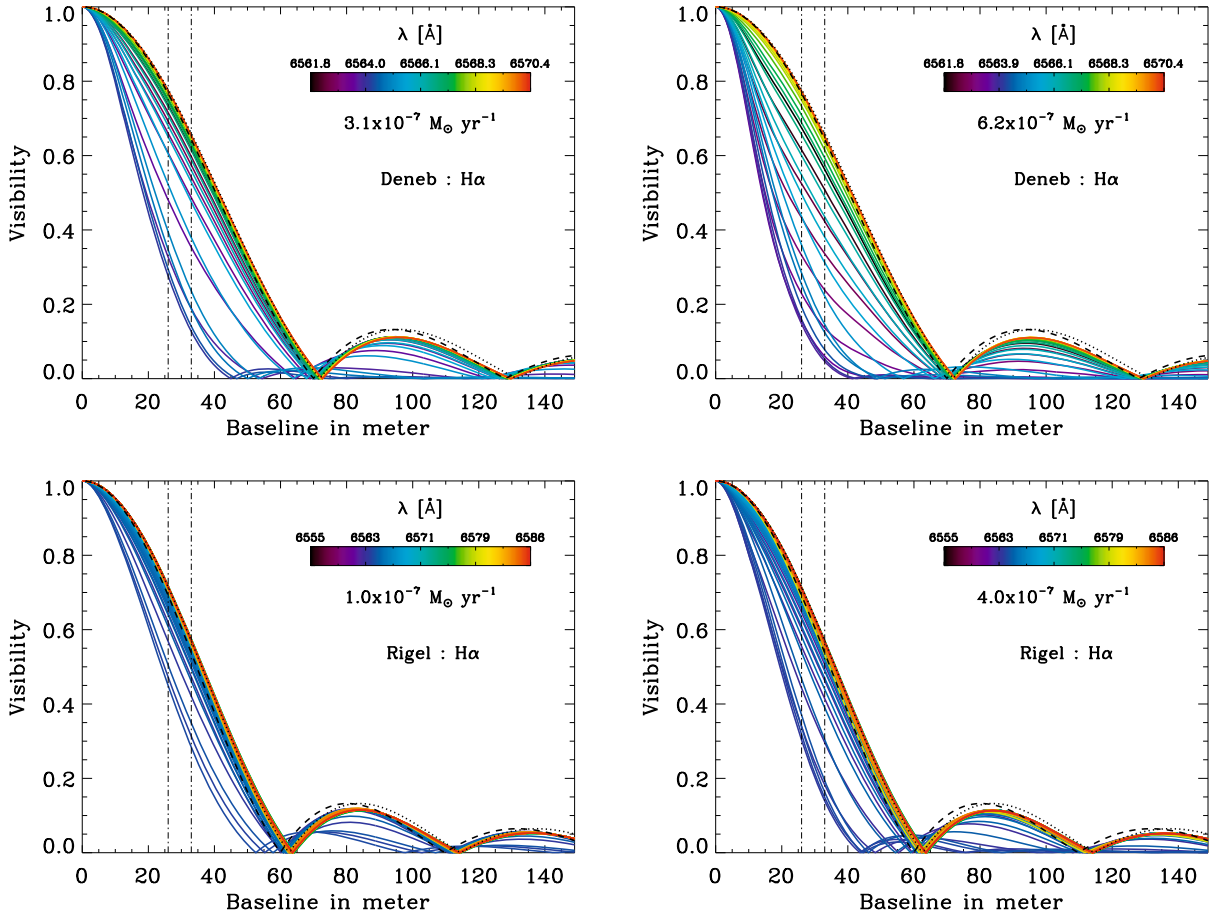

Fig. 7. *Top*: theoretical visibility curves for Deneb, computed at selected wavelengths in the range ~6562–6571 Å, and thus containing the Hα line, and for mass-loss rate values of 3.1×10^{-7} $M_\odot$ yr^{-1} (*left*) and $6.2 \times 10^{-7} M_\odot$ yr^{-1} (*right*). *Bottom*: same as top, but now for Rigel and using mass-loss rate values of 1 (*left*) and 2×10^{-7} $M_\odot$ yr^{-1} (*right*). The dotted and dashed lines correspond to the best UD curves fitting the visible and the near-IR continua, respectively. The range of baselines of the VEGA/CHARA is indicated by two vertical dash-dotted lines.

depending on the atmospheric conditions, and the ability to observe with long baselines. The interpretation of the observations obtained with this instrument might be affected by a mass-loss rate variation in the form of localized inhomogeneities, but probably on a smaller scale than an instrument with a similar accuracy operating in the visible.

The second lobe of the visibility curve is far more sensitive to any fluctuation of the mass-loss rate in the visible than the infrared. The reasons are twofold: a higher sensitivity to limb-darkening effects in the visible, and a more extended continuum-formation region, despite the very limited amount of flux involved (the wind remains in any case optically thin). This can be seen in Fig. 10 as the second lobe of the visibility at 2.2 μm is closer to the uniform disk model than the one at 0.6 μm. Balmer bound-free cross-sections increase from 400 to 800 nm. This causes the continuum photosphere to shift weakly in radius across this wavelength range and also alters the limb-darkening properties of the star. This effect might also be discernible in the MarkIII data (Mozurkewich et al. 2003, Sect.3.1), Deneb appearing smaller at wavelengths close to the Balmer jump, although the baselines were too short to probe the second lobe of the visibility curve. An interferometer able to resolve a hot star up to the second lobe in the visible is very sensitive to the mass-loss rate, even in the case of a very weak wind. In the near-IR, the free-free emission strengthens. Free-free opacities increase at longer wavelengths, increasing the photospheric radius relative to that measured in the visible. Changing the mass-loss rate does not significantly affect the limb-darkening and the temperature scale near the star, thus the location of the extended emission. As a consequence, the free-free emission causes a larger diameter in the near-IR, independently to first order of the mass-loss rate.

4.3. Dependence of the Hα and Si II lines on the mass-loss rate

We then computed the spectrum and the dispersed visibilities in the Hα line at a spectral resolution $R = 30\,000$. We were unable to perform a satisfactory fit to the Hα profile for either Deneb or Rigel, the absorption component being systematically too deep (Fig. 8). This conclusion was reached in many studies, and these profiles could not be reproduced in terms of spherically-symmetric smooth wind models (see for instance Fig. 7 in Markova et al. (2008); Aufdenberg et al. (2002); and Schiller & Przybilla (2008)). In this temperature regime, the models systematically predict profiles in absorption partly filled-in by wind emission, hence only lower limits to the mass-loss rate can be derived by fitting the Hα line.

However, this discrepancy is mitigated by the quality of the visibility fit shown in the upper panel of Fig. 8, which is by far less sensitive to small absorption effects along the line-of-sight.

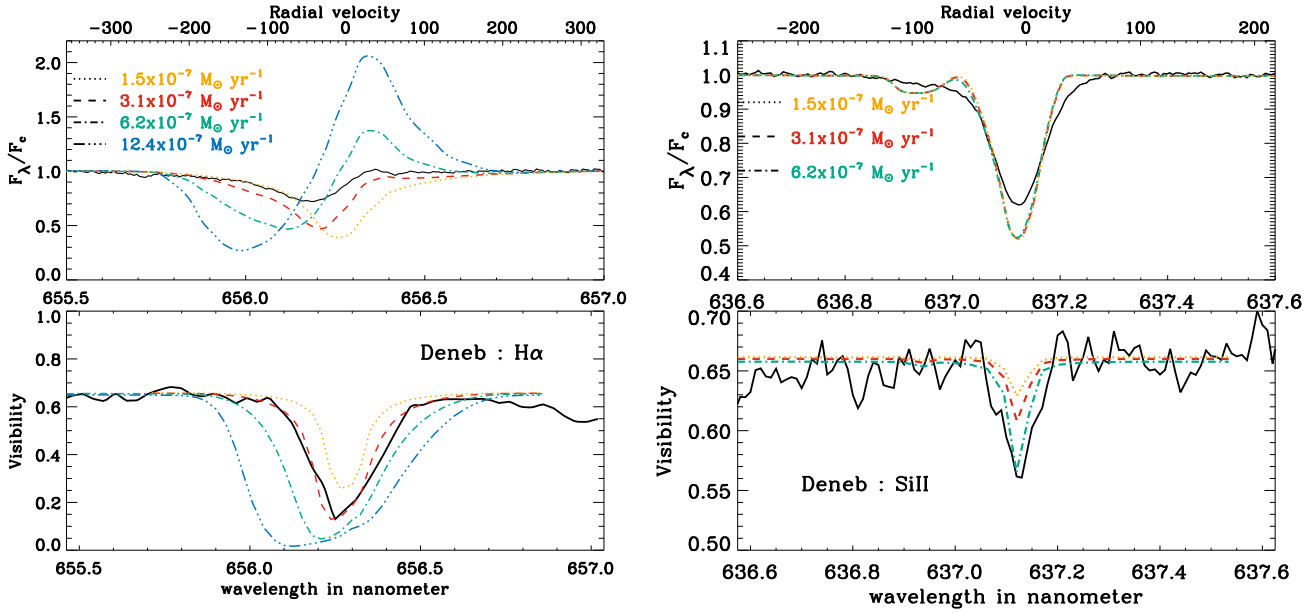

Fig. 8. *Left*: in *the upper panel*, we compare the Hα line profile obtained in July 2008 (black; rectified) of Deneb and the corresponding model predictions for wind mass loss rate of 1.5 (orange), 3.1 (red), 6.2 (green) and 12.4×10^{-7} $M_{\odot}$ yr^{-1} (blue). In *the lower panel*, we give the corresponding dispersed visibility for a nominal baseline of 33 m. *Right*: same as before, but now for SiII 6371 Å.

Changing the mass-loss rate by a large factor of 2–4 has a dramatic impact on the Hα line-formation region, changing the spectrum appearance and the dispersed visibility curve. When using a baseline in the range 26–33 m, there is a relationship between the mass-loss rate and the *FWHM* of the visibility drop in the line that can be approximated by a second-order polynomial in the range considered (1.55 to 12.4×10^{-7} $M_{\odot}$ yr^{-1}). One can see in Fig. 11 that the nominal model of Deneb with a mass-loss rate of 3.1×10^{-7} $M_{\odot}$ yr^{-1} fits the observed visibility curves well. The model *FWHM* of the visibility is 89 km s^{-1} and the observed *FWHM* is 98 ± 3 km s^{-1}. Given the *FWHM*-mass-loss relationship, this would correspond to a mass-loss rate in the range $3.7 \pm 0.2 \times 10^{-7}$ $M_{\odot}$ yr^{-1}. For Rigel, a similar relationship provides a mass-loss rate in the range $1.5 \pm 0.4 \times 10^{-7}$ $M_{\odot}$ yr^{-1}. We have studied the variations in 2008 and 2009 of the visibility profile without detecting any significant variation in the visibility profile, which, translated in a mass-loss rate variation, suggests that the mass-loss rate has not changed by more than 5%.

By comparison, the SiII 6371 Å line is less sensitive to any variation in the mass-loss rate (Fig. 8). The *FWHM* of the simulated line weakly increases from 40 to 43 km s^{-1}, compared to the 2008 VEGA/CHARA measurement of 55 ± 3 km s^{-1}. The *FWHM* of the corresponding model visibility dip are independent of the mass-loss rate, being unchanged at the value 19.5 km s^{-1}and lower than the measured mean value of 29 ± 5 km s^{-1} for the 2008 observations. The depth of the visibility dip fits more accurately the curve with a mass-loss rate of 6.2×10^{-7} rather than the nominal value of 3.1×10^{-7} $M_{\odot}$ yr^{-1} inferred from the Hα line. It is not possible to establish whether this issue is related to a particular event occurring during the 2008 observations, or a permanent situation, or even a bias in the radiative-transfer model.

Despite the lower quality of the interferometric data on Rigel, one can see in Fig. 9 that the model provides a reasonable fit. We note that the CII lines at 6578 Å and 6583 Å in the spectrum of Rigel are also slightly affected by the wind. Their visibility for the VEGA baselines are about 0.5–1% lower than the nearby continuum (using our model predictions), depending on the mass-loss rate. Detecting such a weak signal would require that the accuracy on the differential visibility is about 2–3 times better than the current instrument performance.

4.4. A rough investigation of the morphology of the line-formation regions

The variability in the differential phase signal observed is a clear sign of the stochastic activity of the wind of Deneb. Even though the data secured are partial, one can note that no differential phase signal exceeds 30°, which is impressively large considering that the baseline is limited. In 2008 and in October 2009, the differential phase signal was able to be observed throughout the full line, at a level above 30°. This signal did not appear to be due to an increased level of stochastic "noise" expected from the signature of small, localized clumps, but exhibited a well-structured signature. At other times, the differential signal was only observed close to $\pm v \sin i$, and some patterns were reminiscent of the S-shape signature, originating in a rotating structure.

The radiative transfer models demonstrate that at the inferred mass-loss rate of Deneb, significant emission originates in a circumstellar region of up to 2–4 stellar radii, and that the level of this extended emission depends strongly on the mass-loss rate. We tried to investigate the differential phases with ad hoc approaches using the models as a basis to generate the perturbation. Differential visibilities and phases provide contradictory and stringent constraints. On the one hand, a strong differential phase signal is observed, but on the other hand, the differential visibilities did not vary by more than 5% over the two years of sparse observations. This restricted considerably the size, flux, and location of the perturbation. The emergent flux of the best-fit model was perturbed using a 2D Gaussian as a weighting function. The parameters of the perturbation were its location, *FWHM* and flux ratio compared to the unperturbed model. The

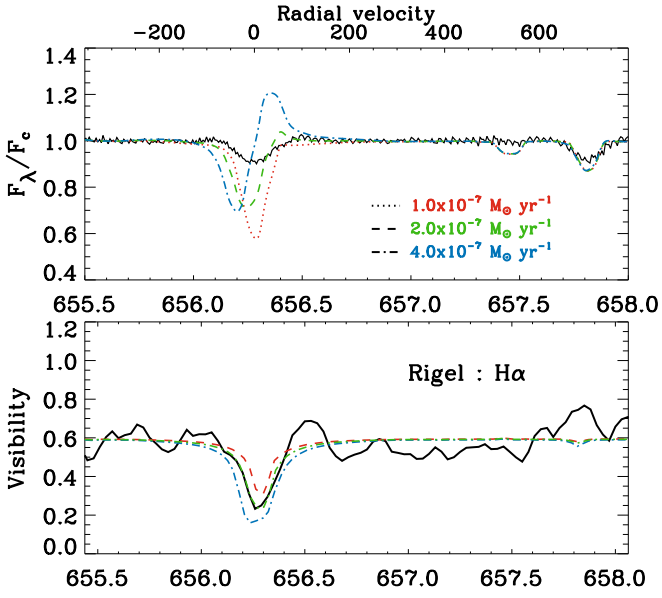

Fig. 9. Same as *the upper panel* of Fig. 8, but now for Rigel.

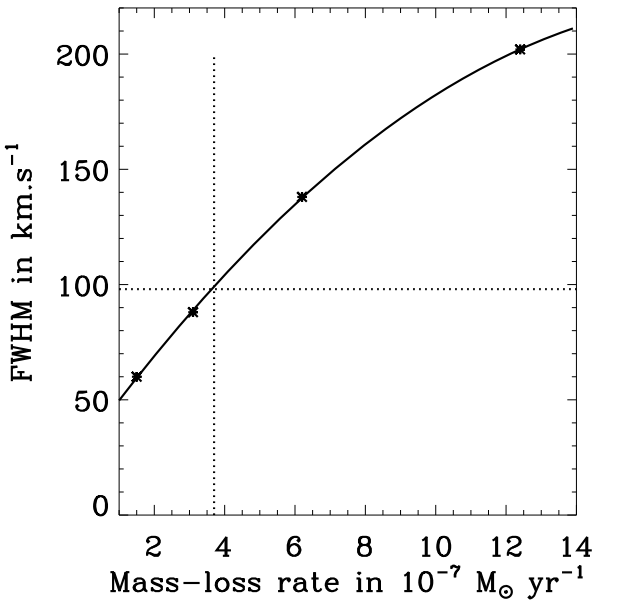

Fig. 11. Variation in the *FWHM* measured from the Hα visibility curves computed with the intensity maps produced by CMGEN, shown here as a function of mass-loss rate and adopting the stellar parameters suitable for Deneb. The adopted baseline is 33 m. For a high mass-loss rate value, the Hα line-formation region is fully resolved, and the *FWHM* of the visibility curve is close to the wind terminal velocity. The dotted lines indicate the mass-loss rate inferred from the VEGA/CHARA measurements.

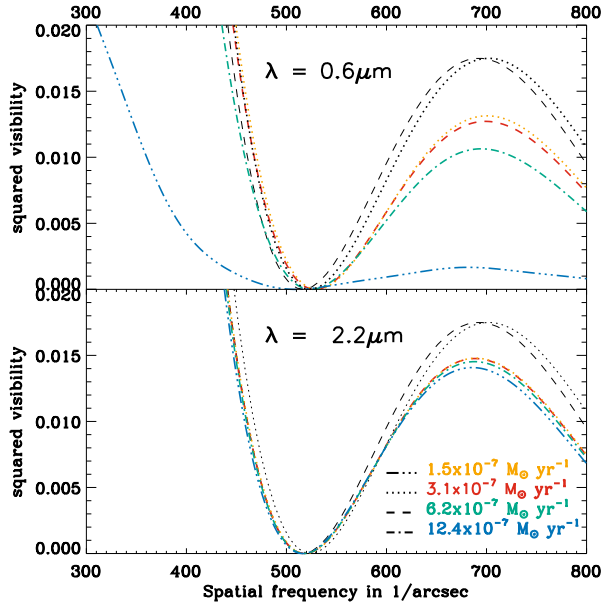

Fig. 10. Synthetic continuum squared-visibility curves at 0.6 μm (*top*) and 2.2 μm (*bottom*) as a function of spatial frequency, and given for wind mass-loss rates of 1.5 (orange), 3.1 (red), 6.2 (green), and 12.4×10^{-7} $M_\odot$ yr^{-1} (blue). The dotted black line corresponds to a uniform disk of 3.32 mas, and the dashed black line to a uniform disk of 3.36 mas.

best parameter range was reached for a perturbation located at 2–3 stellar radii from the star, with a *FWHM* of 0.3–0.7 stellar radii, and a flux contrast of 10–25. One can see in Fig. 12 that the differential visibilities of the perturbed and unperturbed models are similar, whereas a significant differential phase signal is observed. The baseline is aligned in the direction of the perturbation observed in July 2008, i.e. north of the star. This model is also compatible with the differential phases observed with the two other baselines (Fig. 2). Placing the perturbation farther away leads to a phase signal that is far weaker than to the observations, since the line-forming region of the unperturbed model naturally ends at 5–6 stellar radii. This is a limitation of this ad hoc approach. Making the perturbation larger in size, even with a much lower flux contrast leads to a noticeable change in the differential visibilities. The same consequence is reached when putting the perturbation too close to the star. Finally, if the perturbation is too small (i.e. *FWHM* $\leq$ 0.1 mas), the flux contrast required to reach the observed phases is unrealistically high, and such that a significant "binary"-like perturbation in the visibilities should be observed. Finally, this perturbation study suggests that a large temporal variability in the visibility and phase is expected in the visible at high spatial frequencies corresponding to the second lobe of the visibility curve.

Clarke & McLean (1976) and McLean & Clarke (1979) did not detected any significant variation in the polarization of the Hβ and Hα lines in Deneb and Rigel, at a typical level of about 0.1%. Hayes (1986) performed an intensive broadband monitoring in *B*-band polarization of Rigel, revealing a variability at a typical level of 0.2%. The variability pattern in the $Q - U$ plane suggested that the ejection of material was not limited to a plane, and non-radial pulsation were thus proposed as the root cause of these localized ejections. This might be caused by the limited amount of intensive observations. This might also be a consequence, in the case of Deneb, of a small inclination of the rotation axis on the sky. Any large-scale structures orbiting in the equatorial plane would generate a significant polarization variability, without any preferential direction. In addition, no direction appears to be preferred by our observation, though we emphase that such a conclusion is very limited given the stringent limitations in the *uv* coverage.

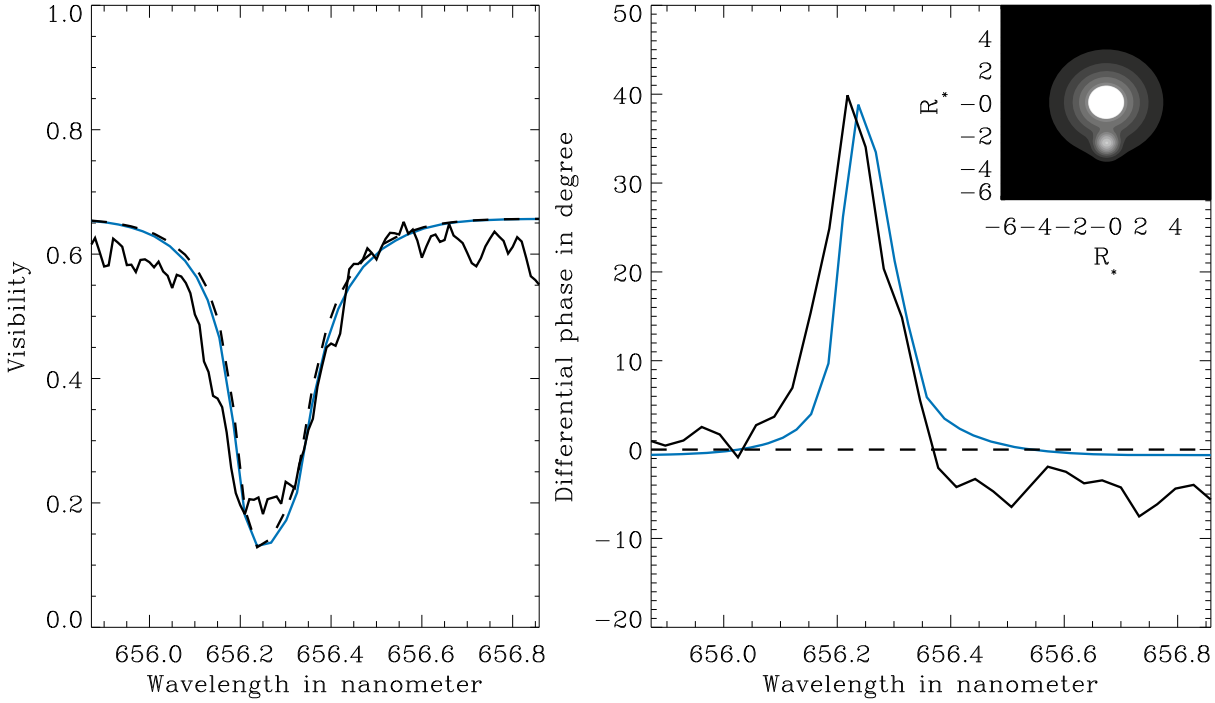

Fig. 12. Comparison on the unperturbed model (dashed lines) with the perturbed model (blue lines, as explained in the text). The thick lines are the observation of July 2008. The parameters of the perturbation are the followings: flux contrast of 20, *FWHM* of 0.5 stellar radius, and position at 2.8 stellar radius south of the star. The insert shows the square root of the perturbed model at the wavelength corresponding to the core of the line, where the signal is maximum.

5. Deneb as a fast rotator

Aufdenberg et al. (2008, 2006a) presented evidence that Deneb is a fast rotator, based on 24 high accuracy FLUOR/CHARA visibilities in the K'-band with projected baselines ranging from 106 m to 310 m, sampling the first and second lobes of the visibility curve. They detected slight departures from a purely spherical model at a level of about 2% in the near-IR, a discovery that had not been anticipated for an AB supergiant. They tentatively fitted the data with a rotating model atmosphere, and demonstrated that despite the low $v \sin i$ of the star, a model at half critical speed, seen nearly pole-on may account for the interferometric observations. A by-product of this fitting process is the determination of crucial parameters in this context, namely the inclination, estimated to be $i = 30°$, and the orientation on the sky of the rotation axis found to be at about PA = 150° east from north. These findings have potentially important implications. In a general context, Deneb would be the first AB supergiant proven to be the descendant of a fast rotator. Support for this interpretation was provided by Schiller & Przybilla (2008). To more clearly interpret the pronounced mixing signature with nuclear-processed matter, these authors proposed that Deneb was probably a fast rotator initially, and is currently evolving to the red-supergiant stage.

In the context of our observations, the consequences on the Hα line-formation region must be evaluated. The Hα line may be affected by a moderate change in wind properties, such as those that occur due to a latitudinal variation in the effective temperature of the star, estimated to be ~700 K (Aufdenberg et al. 2006a). Moreover, as stated by Schiller & Przybilla (2008), hydrogen lines are mainly sensitive to variations in $\log g$.

Neither the VEGA/CHARA data nor the theoretical study presented in this paper can provide definitive support for, or exclude, this interpretation. The Hα variability observed by VEGA/CHARA is related to localized inhomogeneities in the wind of this star. Is not impossible that that these inhomogeneities may affect the continuum forming region in the K band, although is has been shown in Sect. 4.2 that large variations in mass-loss rate are required to significantly affect the second lobe of the visibility curves. Yet, this conclusion is based on the ideal case of a spherical model, although given that the wind is very optically thin in the continuum, those inhomogeneities should not significantly alter the properties of the continuum-formation regions.

The 2008 data arguably provide some support for the fast rotator model. We note that the S1S2 projected baselines were roughly aligned (range of –45/+15 degrees) within the direction of the asymmetry found with CHARA/FLUOR at 150°, i.e. the direction of the pole in the fast rotator model (Aufdenberg et al. 2006a). On the other hand, the Hα differential phases are observed to increase from a baseline roughly aligned to the pole direction at PA = 150°. This may imply that the asymmetry is greater in a direction perpendicular to the pole. On the other hand, the SiII line dispersed visibilities seem deeper in the direction of the pole, suggesting a more extended line-formation region. Moreover, the high mass-loss rate inferred from the fit to the visibilities through the SiII line may also be an indication of a co-latitude dependence of the mass-loss rate. That no evidence of rotation was detected in the differential phases is an additional argument for a low $v \sin i$, and therefore a nearly pole-on configuration for Deneb. These limited observations cannot provide definite conclusions, and the fast-rotator interpretation still needs

to be investigated, both theoretically and observationally. This could be done, for instance, by repeating the FLUOR/CHARA observations to check whether the near-IR interferometric signal has changed or not, or by devoting a full VEGA/CHARA run with more extensive coverage, preferably by using the 3T mode. It would also be of interest to investigate the impact of the fast rotation of Deneb on the Hα and SiII 6371 Å line-forming regions, using a radiative transfer model of a rotating star with a wind.

6. Conclusion

We have presented the first high spatial and spectral observations of two nearby supergiant stars Deneb and Rigel. The Hα line-formation regions were resolved and their angular size was found to be in agreement with an up-to-date radiative transfer model of these stars. The Hα line-forming region appears to be asymmetric and time variable, as expected from the numerous intensive spectral monitoring of AB supergiants reported in the literature. However, the time-monitoring of the dispersed visibilities inferred from the Hα line of Deneb did not provide evidence of mass-loss rate changes above 5% of the mean rate, and the activity observed can be considered most of the time as a second-order perturbation of the wind characteristics. The increased coverage obtained in 2008 provides some evidence of a latitudinal dependence of both the Hα differential phases and the SiII 6371 line differential visibilities. This line was not significantly resolved subsequently. Only two observations of Rigel were secured. An S-shape signal was detected in the Hα differential phase of Rigel, suggesting that the rotation signal is detected. We note that the Hα line profile was almost photospheric at the time of our observations. Observations with a large *uv* coverage may provide, in the case of Rigel, the direction of the rotational axis on the sky and its inclination.

Given the large angular size of Rigel and Deneb, the Hα line-forming region is fully resolved by the interferometer with baselines longer than 50 m, and only the S1S2 baseline of the CHARA array is short enough to permit such an investigation. Therefore, it is not easy to significantly increase the observational effort performed on these stars with such stringent observing restrictions. An extension of this work is possible for sources with an apparent angular diameter between 0.5 and 1.5 mas, that are large enough, but also bright enough to make use of the highest spectral dispersion of the VEGA instrument (limiting magnitude of about 3). This concerns the AB supergiants closer than 1.5 kpc, and the supergiants in the Orion complex ($d \sim 500$ pc) are in this context of particular interest. Simultaneous 3 telescopes recombination would provide much better *uv* coverage than the one presented in this paper. Another interesting possibility is to add to this study several diagnostic lines such as the CaII infrared triplet (849.8 nm, 854.2 nm, 866.2 nm). These resonance lines are highly sensitive to non-LTE effects arising close to the photosphere and may shed some light on the regions were the material is launched.

Acknowledgements. VEGA is a collaboration between CHARA and OCA/LAOG/CRAL/LESIA that has been supported by the French programs PNPS and ASHRA, by INSU and by the règion PACA. The project has obviously taken benefit from the strong support of the OCA and CHARA technical teams. The CHARA Array is operated with support from the National Science Foundation and Georgia State University. We warmly thank Christian Hummel for having provided the MarkIII data. The referee, Mike Ireland helped us by his useful comments to improve this paper significantly. This research has made use of the Jean-Marie Mariotti Center `SearchCal` service[2] co-developed by FIZEAU and LAOG, and of CDS Astronomical Databases SIMBAD and VIZIER[3]. M.B.F. acknowledges Conselho Nacional de Desenvolvimento Científico e Tecnológico (CNPq-Brazil) for the post-doctoral grant.

References

Aerts, C., Puls, J., Godart, M., & Dupret, M. 2009, A&A, 508, 409
Aufdenberg, J. P., Hauschildt, P. H., Baron, E., et al. 2002, ApJ, 570, 344
Aufdenberg, J. P., Mérand, A., Ridgway, S. T., et al. 2006a, BAAS, 38, 84
Aufdenberg, J. P., Morrison, N. D., Hauschildt, P. H., & Adelman, S. J. 2006b, in Astrophysics in the Far Ultraviolet: Five Years of Discovery with FUSE, ed. G. Sonneborn, H. W. Moos, & B.-G. Andersson, ASP Conf. Ser., 348, 124
Aufdenberg, J. P., Ludwig, H., Kervella, P., et al. 2008, in The Power of Optical/IR Interferometry: Recent Scientific Results and 2nd Generation, ed. A. Richichi, F. Delplancke, F. Paresce, & A. Chelli, 71
Berio, P., Stee, P., Vakili, F., et al. 1999, A&A, 345, 203
Bonneau, D., Clausse, J., Delfosse, X., et al. 2006, A&A, 456, 789
Bychkov, V. D., Bychkova, L. V., & Madej, J. 2003, A&A, 407, 631
Cantiello, M., Langer, N., Brott, I., et al. 2009, A&A, 499, 279
Clarke, D., & McLean, I. S. 1976, MNRAS, 174, 335
Clausse, J. 2008, SPIE Conf., 7019
Cranmer, S. R. 2009, ApJ, 701, 396
Danezis, E., Lyratzi, E., Popović, L. Č., Dimitrijević, M. S., & Antoniou, A. 2009, New Astron. Rev., 53, 214
Dessart, L., & Chesneau, O. 2002, A&A, 395, 209
Dessart, L., & Hillier, D. J. 2005, A&A, 437, 667
Evans, C. J., & Howarth, I. D. 2003, MNRAS, 345, 1223
Gautschy, A. 1992, MNRAS, 259, 82
Gautschy, A. 2009, A&A, 498, 273
Hayes, D. P. 1986, ApJ, 302, 403
Henrichs, H. F., Neiner, C., & Geers, V. C. 2003, in A Massive Star Odyssey: From Main Sequence to Supernova, ed. K. van der Hucht, A. Herrero, & C. Esteban, IAU Symp., 212, 202
Hillier, D. J., & Miller, D. L. 1998, ApJ, 496, 407
Kaufer, A. 1998, ed. R. E. Schielicke, Rev. Mod. Astron., 11, 177
Kaufer, A., Stahl, O., Wolf, B., et al. 1996a, A&A, 314, 599
Kaufer, A., Stahl, O., Wolf, B., et al. 1996b, A&A, 305, 887
Kaufer, A., Stahl, O., Wolf, B., et al. 1997, A&A, 320, 273
Koechlin, L., Lawson, P. R., Mourard, D., et al. 1996, Appl. Opt., 35, 3002
Kudritzki, R. P., Puls, J., Lennon, D. J., et al. 1999, A&A, 350, 970
Kudritzki, R., Urbaneja, M. A., Bresolin, F., et al. 2008, ApJ, 681, 269
Le Bouquin, J., Absil, O., Benisty, M., et al. 2009, A&A, 498, L41
Lucy, L. B. 1976, ApJ, 206, 499
Markova, N., & Puls, J. 2008, A&A, 478, 823
Markova, N., Prinja, R. K., Markov, H., et al. 2008, A&A, 487, 211
McLean, I. S., & Clarke, D. 1979, MNRAS, 186, 245
Morel, T., Marchenko, S. V., Pati, A. K., et al. 2004, MNRAS, 351, 552
Morrison, N. D., Rother, R., & Kurschat, N. 2008, in Clumping in Hot-Star Winds, ed. W.-R. Hamann, A. Feldmeier, & L. M. Oskinova, 155
Mourard, D., Clausse, J. M., Marcotto, A., et al. 2009, A&A, 508, 1073
Mozurkewich, D., Armstrong, J. T., Hindsley, R. B., et al. 2003, AJ, 126, 2502
Neiner, C., Gutiérrez-Soto, J., Baudin, F., et al. 2009, A&A, 506, 143
Paddock, G. F. 1935, Lick Observatory Bulletin, 17, 99
Puls, J., Vink, J. S., & Najarro, F. 2008, A&ARv, 16, 209
Rivinius, T., Stahl, O., Wolf, B., et al. 1997, A&A, 318, 819
Rzaev, A. K. 2008, Astrophys. Bull., 63, 23
Schiller, F., & Przybilla, N. 2008, A&A, 479, 849
Schnerr, R. S., Henrichs, H. F., Neiner, C., et al. 2008, A&A, 483, 857
Stee, P. 1996, A&A, 311, 945
ten Brummelaar, T. A., McAlister, H. A., Ridgway, S. T., et al. 2005, ApJ, 628, 453
Vakili, F., Mourard, D., Stee, P., et al. 1998, A&A, 335, 261
van Leeuwen, F. 2007, A&A, 474, 653
Verdugo, E., Talavera, A., Gómez de Castro, A. I., & Henrichs, H. F. 2003, in A Massive Star Odyssey: From Main Sequence to Supernova, ed. K. van der Hucht, A. Herrero, & C. Esteban, IAU Symp., 212, 255

[2] Available at http://www.jmmc.fr/searchcal
[3] Available at http://cdsweb.u-strasbg.fr/